

Calculation of the rate of nuclear excitation by electron transition in an ^{84m}Rb plasma under the hypothesis of local thermodynamic equilibrium using a multiconfiguration Dirac-Fock approach

David Denis-Petit,^{1,2,*} Gilbert Gosselin,² Fazia Hannachi,¹ Medhi Tarisien,¹ Thomas Bonnet,¹ Maxime Comet,² Franck Gobet,¹ Maud Versteegen,¹ Pascal Morel,² Vincent Méot,² and Iolanda Matea³

¹Université de Bordeaux, CNRS-IN2P3, CENBG, F-33175 Gradignan, France

²CEA, DAM/DIF, F-91297 Arpajon, France

³IPN, Université Paris Sud, F-91400 Orsay, France

(Received 21 March 2017; published 2 August 2017)

One promising candidate for the first detection of nuclear excitation in plasma is the 463-keV, 20.26-min-lifetime isomeric state in ^{84}Rb , which can be excited via a 3.5-keV transition to a higher lying state. According to our preliminary calculations, under specific plasma conditions, nuclear excitation by electron transition (NEET) may be its strongest excitation process. Evaluating a reliable NEET rate requires, in particular, a thorough examination of all atomic transitions contributing to the rate under plasma conditions. We report the results of a detailed evaluation of the NEET rate based on multiconfiguration Dirac Fock (MCDF) atomic calculations, in a rubidium plasma at local thermodynamic equilibrium with a temperature of 400 eV and a density of 10^{-2} g/cm³ and based on a more precise energy measurement of the nuclear transition involved in the excitation.

DOI: [10.1103/PhysRevC.96.024604](https://doi.org/10.1103/PhysRevC.96.024604)

I. INTRODUCTION

Nuclear excitation by electronic transition (NEET) is the inverse process of internal conversion between bound atomic states which was first demonstrated in ^{125}Te [1]. It is a resonant process in which an electron on a weakly bound shell decays down to an inner shell. The energy released in this process is transferred to the nucleus of the same atomic system. It may take place if the energies of the atomic and nuclear transitions are close enough and if the two transitions share the same multipolarity. It was first suggested by Morita for the excitation of the level at 13 keV in ^{235}U [2] and later demonstrated in experiments where nuclear ground-state targets of ^{197}Au , ^{189}Os , ^{193}Ir , and ^{237}Np were irradiated with photon beams [3–6]. However, it has never been evidenced in plasma, where it is predicted to be the dominant nuclear excitation process under specific conditions of plasma temperature and density [7,8].

The main difficulty in observing such a process lies in the detection of a nuclear transition in the high background due to plasma emissions. To overcome this difficulty the plasma target can be a long-lived nuclear excited state whose induced deexcitation in plasma will be signaled by the detection of γ -rays with energies higher than the plasma x-ray emission. The $J^\pi = 6^-, T_{1/2} = 20.26(3)$ min isomeric state of the unstable ^{84}Rb nucleus lies at an excitation energy of 463 keV, about 3 keV lower than the $J^\pi = 5^-, T_{1/2} = 9$ ns state [9]. Thus, upon providing it an energy of only about 3 keV, 466 keV of the nuclear excitation energy might be released in the plasma within a few tens of nanoseconds.

In a plasma at local thermodynamic equilibrium (LTE) with a temperature of $T = 400$ eV and a density of $\rho = 10^{-2}$ g/cm³, the $6^- \rightarrow 5^-$ excitation is predicted to take place by NEET in calculations in which rubidium ions in

plasma are described with the relativistic average atom model (RAAM) [10]. However, one may question the relevance of the RAAM model for describing a resonant process, for two reasons: first, the use of average configurations at temperatures where the number of real configurations, although high, may not be high enough to average out all the atomic properties; and, second, the RAAM average configuration is used, which may be quite different from real configurations able to induce a NEET transition. Another significant issue is the large uncertainty, a few hundred eV, in the nuclear transition energy.

As a first step towards the prediction of more precise ^{84}Rb nuclear excitation rates in plasma, we have developed a numerical method based on multiconfiguration Dirac-Fock (MCDF) [11] calculations to describe highly charged Rb ions in plasma [12] and we have performed experiments to measure more precisely the nuclear transition energy involved in the NEET process [13]. The most restrictive hypothesis in our study is to consider a laser-created plasma at LTE. Indeed, this kind of plasma is generally non-LTE and the atomic physics involved is more complex. However, we have already shown that some spectroscopic properties of a non-LTE plasma can be reproduced using an LTE plasma with a similar charge state distribution [12].

In this paper, we present new NEET excitation rates for the ^{84}Rb 6^- isomeric state in a plasma at an LTE temperature of $T = 400$ eV and a density of $\rho = 10^{-2}$ g/cm³. The latter corresponds to the critical density for a $\lambda = 1.06$ μm laser.

II. EXPRESSION OF THE NEET RATE IN AN LTE PLASMA USING MULTICONFIGURATION DIRAC-FOCK CALCULATIONS

A. The NEET probability

In the initial state of a NEET process the atom is in an excited level (labeled i) at energy E_i and the nucleus is in a

*petit@cenbg.in2p3.fr

level (labeled 1) at energy E_1 . The final state corresponds to the atom in a final level f at energy $E_f < E_i$ and the nucleus in an excited level labeled 2 at energy $E_2 > E_1$.

The width of the initial or final NEET state is expressed as a sum over the widths of the atomic and nuclear levels involved. Usually, nuclear level widths are negligible in comparison to atomic level ones. For the ^{84}Rb nucleus the widths of the 5^- and 6^- levels are 5.1×10^{-8} and 3.8×10^{-19} eV, respectively [9]. For plasma densities higher than 10^{-2} g/cm 3 , the collisional atomic level widths with typical values of a few meV are dominant. Therefore, only the atomic state widths (initial Γ_i , final Γ_f) are taken into account in our calculations.

Theoretical calculations of NEET rates have been the subject of numerous publications since the first description by Morita [2]. In 1976, Grechukhin and Soldatov demonstrated that the interaction Hamiltonian proposed by Morita was wrong [14]. In 1992, Tkalya described the NEET process with the help of quantum electrodynamics [15]. In 1999, Harston and Chemin published an overview of the different nuclear excitation processes in plasma [16]. In the case of ^{235}U , with the help of an MCDF code they calculated the NEET rate for three atomic transitions suggested by Tkalya [15] to contribute the most to the process. In this paper, the NEET probability calculated by Tkalya has been slightly modified to correct for the erroneous definition of the nuclear reduced transition probability as explained by Harston in Ref. [17]. Harston has presented all available NEET experimental data and discussed the corresponding theoretical evaluations. In 2004, Morel *et al.* proposed a description of the NEET process in the framework of the formal theory of reactions [8], based on a decay theory developed by Golberger and Watson [18]. The NEET probability proposed by these authors reaches an asymptotic value $P_{\text{NEET}}^{i1 \rightarrow f2}(t \rightarrow \infty)$ with a characteristic time $\tau_{\infty}^{i1 \rightarrow f2}$ given by

$$\tau_{\infty}^{i1 \rightarrow f2} = \frac{\hbar}{2} \left(\frac{1}{\Gamma_i} + \frac{1}{\Gamma_f} \right), \quad (1)$$

$$P_{\text{NEET}}^{i1 \rightarrow f2}(t \rightarrow \infty) = \left(1 + \frac{\Gamma_f}{\Gamma_i} \right) \frac{|R_{i1,f2}|^2}{(\delta_{i1,f2})^2 + \left(\frac{\Gamma_i + \Gamma_f}{2} \right)^2}, \quad (2)$$

where $|R_{i1,f2}|^2$ is defined as a sum over the final atomic and nuclear magnetic substates of the squared atom-nucleus coupling matrix element averaged over the initial magnetic and nuclear ones (see the Appendix). The energy mismatch $\delta_{i1,f2}$ is defined as

$$\delta_{i1,f2} = \Delta E_{if} - \Delta E_{12}, \quad (3)$$

where $\Delta E_{if} = E_i - E_f$ and $\Delta E_{12} = E_2 - E_1$ are the atomic and nuclear transition energy differences, respectively.

This asymptotic NEET probability is identical to the one published by Harston [17]. In the following, we consider an ^{84m}Rb plasma produced with a nanosecond-duration laser pulse. Under this condition, the NEET probability reaches its asymptotic value after about 1 ps (see Sec. III C 2). We have therefore used only this asymptotic value in the calculations and removed the time dependence in the equations to lighten the notations: $P_{\text{NEET}}^{i1 \rightarrow f2}(t \rightarrow \infty) = P_{\text{NEET}}^{i1 \rightarrow f2}$.

Recently, Dzyublik used the collision theory in combination with quantum electrodynamics to express the NEET cross section [19,20]. In particular, he described the behavior of the NEET cross section around the photoabsorption threshold in order to explain the NEET fine structure observed by Kishimoto *et al.* [21]. This behavior is modeled by a NEET edge function $F(E)$ which depends on the photon energy E . The NEET probability is the product of the asymptotic NEET probability [Eq. (2)] and this edge function. Far from resonance, $F(E) \rightarrow 1$ and the NEET probability is the same as Eq. (2). In our calculations, the impact of this accurate description of the NEET around the absorption threshold is expected to be weak in comparison to the other sources of uncertainties and therefore we consider $F(E) = 1$ in the following. Moreover, as the description of the atomic state formation in plasma is more complex than in the case of a solid target (only photoionization was considered by Dzyublik), we do not take into account this stage of the NEET process in our calculations.

The expression of the atom-nucleus coupling term $|R_{i1,f2}|^2$ depends on the basis used to express the atomic and nuclear states. To select the atomic transitions which can match the nuclear one, we used the MCDF code developed by Bruneau [11]. The MCDF method is described in detail in several papers (see, for example, [22–26]). In each MCDF calculation, the Dirac-Fock equation is solved to determine the atomic eigenstates using the average level method. An eigenstate $|J_i M_i \Pi_i\rangle$ is characterized by its energy, parity Π_i , total angular momentum J_i and the projection M_i of the total angular momentum. It is expressed as a linear combination of configuration state functions (CSFs) $|v_t J_t M_t \Pi_t\rangle$,

$$|J_i M_i \Pi_i\rangle = \sum_t c_{it} |v_t J_t M_t \Pi_t\rangle, \quad (4)$$

where c_{it} are real coefficients and v_t represents all the other quantum numbers required to describe a CSF unambiguously. A CSF is a linear combination of Slater's determinants, which are built with the atomic orbitals $|n\kappa jm\rangle$ of the electronic configurations used as inputs in MCDF calculations. An orbital is described by the principal quantum number n , the total angular momentum j and its projection m , and the relativistic quantum number κ related to the total angular momentum j by $j = |\kappa| - \frac{1}{2}$.

In the $|JM\Pi\rangle$ basis and for one πL ($\pi = E$ or M) transition, the term $|R_{i1,f2}|^2$ is given by (see the Appendix for more details)

$$|R_{i1,f2}|^2 = \frac{4\pi e^2}{2J_i + 1} \frac{(k_{12})^{2L+2}}{[L(2L+1)]!^2} B_{I_1 \rightarrow I_2}(\pi L) \left| \sum_{it'} \sum_{kk'} \sqrt{2j_{k'} + 1} c_{it'} c_{ft} a_{t'k'k} \left\langle j_{k'} L \frac{1}{2} 0 \left| j_k \frac{1}{2} \right\rangle M_{k'k}^e(\pi L) \right|, \quad (5)$$

where e is the electric charge, L is the multipolarity of the considered atomic and nuclear transitions, k_{12} is the wave vector of the nuclear transition, $B_{I_1 \rightarrow I_2}(\pi L)$ is the reduced transition probability of the nuclear transition, $\langle j_k L \frac{1}{2} 0 | j_k \frac{1}{2} \rangle$ is a Clebsch-Gordan coefficient, and $a_{t' t k k'}$ is a coefficient which links the reduced matrix element of a tensor operator O in the CSF basis and the reduced matrix element in the orbital basis (see [24] for more details):

$$\langle v_{t'} J_{t'} \Pi_{t'} \parallel O \parallel v_t J_t \Pi_t \rangle = \sum_{kk'} a_{t' t k k'} \langle n_{k'} \kappa_{k'} j_{k'} \parallel O \parallel n_k \kappa_k j_k \rangle. \quad (6)$$

In Eq. (5), $M_{k'k}^e(\pi L)$ is the electronic matrix element between the orbitals k and k' . For an electric transition EL , $M_{k'k}^e(EL)$ is given by

$$\begin{aligned} M_{k'k}^e(EL) = & \int_{r=0}^{+\infty} (L[P_k(r)P_{k'}(r) + Q_k(r)Q_{k'}(r)] \\ & \times h_L(k_{12}r) + [(\kappa_k - \kappa_{k'} - L)P_k(r)Q_{k'}(r) \\ & + (\kappa_k - \kappa_{k'} + L)P_{k'}(r)Q_k(r)]h_{L-1}(k_{12}r))dr, \end{aligned} \quad (7)$$

where $P_k(r)$ and $Q_k(r)$ are the large and small components of the wave function of subshell k , respectively, and h_L is the Hankel's function of the first kind and of L order. In the case of a magnetic transition ML , $M_{k'k}^e(ML)$ is written as

$$\begin{aligned} M_{k'k}^e(ML) = & (\kappa_k + \kappa_{k'}) \int_{r=0}^{+\infty} ([P_k(r)Q_{k'}(r) \\ & + P_{k'}(r)Q_k(r)]h_L(k_{12}r))dr. \end{aligned} \quad (8)$$

Fully taking into account the configuration interaction (CI) in an MCDF calculation would require making a calculation with all significant atomic configurations. This is obviously out of reach for even the fastest computers currently available. Two more realistic approaches can be envisaged. CI within nonrelativistic configurations groups in a single MCDF calculation all atomic configurations having the same number of electrons in the same (n, l) subshells. As the gain in accuracy with this technique is small for our purpose [12], we have adopted a simpler approach considering only the initial and final (n, l, j) configurations. In this case, for an atomic transition $\alpha \rightarrow \beta$ between the initial $(n_\alpha, l_\alpha, j_\alpha)$ relativistic subshell and the final $(n_\beta, l_\beta, j_\beta)$ one, Eq. (5) is simplified as the sum over the subshells k and k' reduces to one term because only the $a_{t' t \beta \alpha}$ coefficient is nonvanishing. Thus, the coupling term $|R_{i1, f2}|^2$ becomes

$$\begin{aligned} |R_{i1, f2}|^2 = & 4\pi e^2 \left(\sum_{t'} c_{it'c_{ft}a_{t'\beta\alpha}} \right)^2 \frac{2j_\beta + 1}{2J_i + 1} \\ & \times \frac{(k_{12})^{2L+2}}{[L(2L+1)!!]^2} \left\langle j_\beta L \frac{1}{2} 0 \left| j_\alpha \frac{1}{2} \right. \right\rangle^2 \\ & \times |M_{\beta\alpha}^e(\pi L)|^2 B_{I_1 \rightarrow I_2}(\pi L). \end{aligned} \quad (9)$$

By applying the inversion rules of the Clebsch-Gordan coefficients, Eq. (9) can be written as

$$\begin{aligned} |R_{i1, f2}|^2 = & 4\pi e^2 \left(\sum_{t'} c_{it'c_{ft}a_{t'\beta\alpha}} \right)^2 \frac{2j_\alpha + 1}{2J_i + 1} \\ & \times \frac{(k_{12})^{2L+2}}{[L(2L+1)!!]^2} \left\langle j_\alpha L \frac{1}{2} 0 \left| j_\beta \frac{1}{2} \right. \right\rangle^2 \\ & \times |M_{\beta\alpha}^e(\pi L)|^2 B_{I_1 \rightarrow I_2}(\pi L). \end{aligned} \quad (10)$$

If we adopt the same convention as Harston and Chemin [16] for the electronic matrix element, which is equal to $M_{\beta\alpha}^e(\pi L)$ divided by L , expression (10) is identical to equation (9) in their paper. This indicates that we have used the same treatment of the CI.

B. NEET rate in plasma

In a nonplasma target, the atomic state f is always the ground state and the NEET probability rate is expressed as the product of the atomic hole formation $\lambda_{f \rightarrow i}$ and the NEET probability $P_{\text{NEET}}^{i1 \rightarrow f2}$ [19,20,27,28].

In a plasma, the excited atomic states are also populated by several processes (photoexcitation, electron collisions, the Auger effect, etc.). The probability that an atomic state i of a charge state Q is populated, P_i^Q , depends on the plasma thermodynamic conditions. If we consider an LTE plasma at a temperature T (expressed in energy units), the probability P_i^Q is evaluated by a partition function,

$$P_i^Q = \frac{g_i \exp(-E_i/T)}{\sum_j g_j \exp(-E_j/T)}, \quad (11)$$

where g_i and E_i are, respectively, the statistical weight and the energy of state i . The NEET excitation rate from an excited atomic state i to a less excited state f can be expressed in an LTE plasma by analogy with the nonplasma case by taking into account the occupation probability of state f ,

$$\lambda_{\text{NEET}}^{i1 \rightarrow f2} = P_Q P_f^Q \lambda_{f \rightarrow i} P_{\text{NEET}}^{i1 \rightarrow f2}, \quad (12)$$

where P_Q is the fraction of the charge state Q . Under the LTE hypothesis, excitation $\lambda_{f \rightarrow i}$ and deexcitation $\lambda_{i \rightarrow f}$ rates are related by [29]

$$\frac{\lambda_{f \rightarrow i}}{\lambda_{i \rightarrow f}} = \frac{g_i}{g_f} e^{(E_f - E_i)/T} = \frac{P_i^Q}{P_f^Q} \quad (13)$$

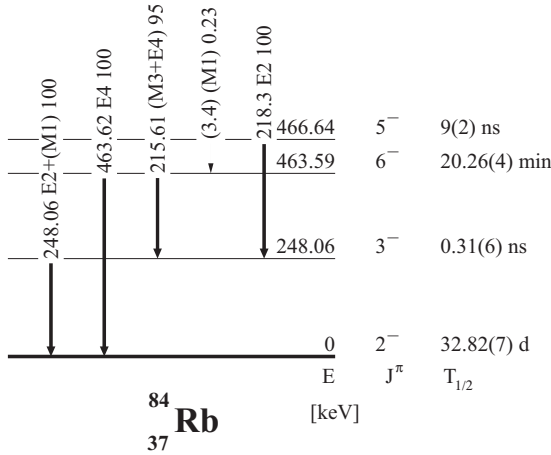
$$\Rightarrow \lambda_{i \rightarrow f} P_i^Q = \lambda_{f \rightarrow i} P_f^Q. \quad (14)$$

By introducing (14) into (12), the NEET excitation rate can be expressed with the deexcitation rate of the excited state i and its occupation probability:

$$\lambda_{\text{NEET}}^{i1 \rightarrow f2} = P_Q P_i^Q \lambda_{i \rightarrow f} P_{\text{NEET}}^{i1 \rightarrow f2}. \quad (15)$$

As a great number of atomic lines may contribute to the NEET process in a plasma, the total NEET rate λ_{NEET} is obtained as a sum over all corresponding atomic lines $i \rightarrow f$:

$$\lambda_{\text{NEET}} = \sum_Q \sum_{i \rightarrow f} P_Q P_i^Q \lambda_{i \rightarrow f} P_{\text{NEET}}^{i1 \rightarrow f2}. \quad (16)$$

FIG. 1. Partial level scheme of ^{84}Rb [9].

This expression has been used for the previous NEET rate estimations in plasmas [8,16,30]. As reported in Ref. [8], the atomic deexcitation rate can be related to the state width Γ_i by $\lambda_{i \rightarrow f} = \frac{\Gamma_i}{\hbar}$.

III. EVALUATION OF THE ^{84m}Rb EXCITATION RATE IN A PLASMA UNDER THE LTE HYPOTHESIS

The NEET excitation rate in plasma is expressed as a sum over all contributing πL atomic lines in the plasma (see the Appendix). MCDF calculations for all atomic configurations and transitions leading to these lines are required to evaluate the atomic wave functions. In these calculations, the ions are isolated and the plasma temperature and density are not taken into account. The description of the plasma, considered at LTE, is thus introduced *a posteriori*. In practice, these calculations are performed only for selected charge states, atomic transitions and configurations most contributing to the rate. In this work, these are selected using the RAAM, which allows fast excitation rate calculations [31]. In this model, all the atoms of the plasma are replaced by one average atom. Its properties, such as orbital occupations, charge state, and wave functions, are averages over all the ions present in the plasma. The average transition energies are calculated as described in [32]. The RAAM is implemented in the ISOMEX code [7,32–34]. This has been used for the first calculations of the ^{84m}Rb excitation rates in plasma [10].

NEET rate computations with the MCDF are performed at the temperature $T = 400$ eV, which corresponds to the maximum of the NEET rate in the ISOMEX calculations, and at a plasma density of 10^{-2} g/cm³. In the following, the different contributions to the NEET rate [Eq. (16)] are evaluated and discussed.

A. Characterization of the $5^- \rightarrow 6^-$ transition

1. Measurement of its transition energy

A partial level scheme of the ^{84}Rb nucleus is shown in Fig. 1. The energy of the $5^- \rightarrow 6^-$ transition has never been measured. It has been deduced from other transition energies or level energy differences. The values reported in the literature

TABLE I. Published energies for the $5^- \rightarrow 6^-$ transition in ^{84}Rb [9].

$5^- \rightarrow 6^-$ transition energy (keV)	Reference
4	Han <i>et al.</i> [35]
3.31 (31)	Schwengner <i>et al.</i> [36]
3.4	Doring <i>et al.</i> [37]

are listed in Table I. Depending on the estimation method, the transition energy lies between 3.31 and 4 keV, with associated uncertainties of a few hundred eV. The last evaluation of these data occurred in 2009 and recommended a value of 3.4 keV [9]. The energy of this nuclear transition is a key parameter of the NEET excitation rate. Therefore, prior to our NEET rate evaluation, we have undertaken the indirect measurement of this transition energy with a higher accuracy.

The energy of the $5^- \rightarrow 6^-$ transition was measured as the difference between the energy of the $5^- \rightarrow 3^-$ and that of the $6^- \rightarrow 3^-$ transitions.

First, the energy of the 215.61-keV γ line was more precisely measured in the off-line deexcitation of the 6^- isomeric state populated in $^{85}\text{Rb}(\gamma, n)$ reactions. These were induced by Bremsstrahlung photons produced at the ELSA electron beam facility of the CEA/DAM/DIF research center. After irradiation the natural rubidium sample was set in front of a properly shielded low-background Ge detector and counted [38]. Special attention was paid to the stability of the Ge power supply and amplifier gain. ^{152}Eu and ^{133}Ba γ -ray sources were measured simultaneously with the Rb activated samples. Besides the europium and barium standard lines, rubidium lines emitted in the deexcitation of the ^{84m}Rb 6^- isomeric state are visible in the spectrum displayed in Fig. 2. Analysis of the Ge spectra was done using the Radware software package [39]. We have used the precisely known energies of the europium and barium lines to calibrate the Ge spectra accumulated over different runs [40,41]. The average values of the energies of the Rb lines of interest

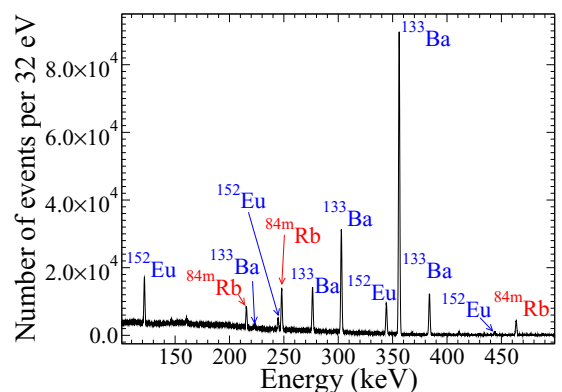


FIG. 2. Typical spectrum recorded during the ELSA experiment. Europium and barium sources were counted together with the rubidium sample.

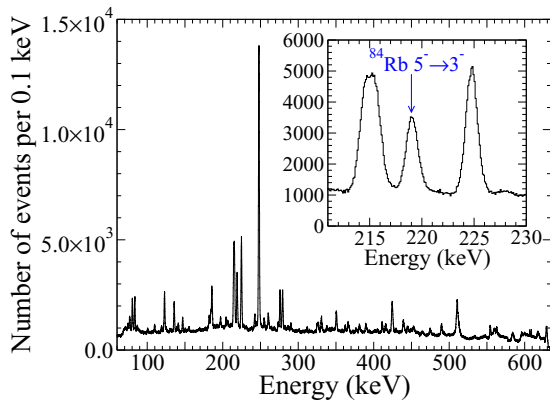


FIG. 3. Typical spectrum recorded during the Orsay experiment. The line at 248 keV is the $3^- \rightarrow 2^-$ transition to the ground state of ^{84}Rb . Inset: Zoom-in centered on the $5^- \rightarrow 3^-$ γ line of interest.

measured over 10 of these runs are 215.601(1), 248.013(2), and 463.618(3) keV, respectively. The given uncertainties account for the published uncertainties in the calibration lines and the statistical uncertainties as well as the ones related to the fitting procedure used in the line centroid evaluation.

Second, the energy of the 218.3-keV γ line was re-measured online in an experiment performed at the Orsay Tandem accelerator using the ORGAM multidetector array composed of 12 Compton suppressed high-volume (70 %) Ge detectors. The high-spin states of ^{84}Rb were populated via $^{76}\text{Ge}(^{11}\text{B}, 3n)$ reactions at a beam energy of 40 MeV. In order to avoid Doppler broadening of the γ lines of interest, 99% enriched ^{76}Ge targets deposited on thick gold backing were used. In order to isolate the 218.3-keV line of interest, γ - γ coincidences were recorded. A total projection of the recorded γ - γ coincidence events is shown in Fig. 3. The inset shows a zoom-in on the energy region of interest for our purpose. The Ge online spectra were precisely calibrated using the well isolated Rb lines at 248.013(2) and 463.618 (3) keV measured previously and the 278.010(50)-keV gold line. The centroid of the line tabulated as 218.3(2) keV was measured at 219.099(5) keV, allowing us to deduce the new value of 3.498(6) keV for the $5^- \rightarrow 6^-$ transition energy. This new value is about 500 eV higher than the one used for previous NEET calculations [10]. As NEET is a resonant process, this new transition energy will have an important impact on its rate and therefore all previous NEET rate estimations should be reevaluated.

2. Determination of its electromagnetic nature and reduced transition probability

An $M1$ electromagnetic nature is assumed for the $5^- \rightarrow 6^-$ nuclear transition in the last evaluation [9]. The associated $M1$ reduced transition probability is not precisely known and no error bars are given on the published value of 0.08 W.u. [9]. Shell model calculations using the effective interaction of Honma *et al.* for the $f_{5/2}$ - $g_{9/2}$ space predict a value of 0.116 W.u. [42,43], which is not too far from the published one. We have used the published value and considered a maximal

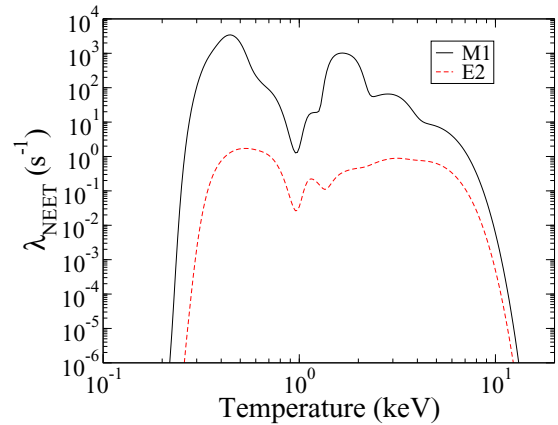


FIG. 4. NEET rate for the $6^- \rightarrow 5^-$ transition calculated with ISOMEX as a function of the plasma temperature for the $M1$ and $E2$ components. The plasma density is 10^{-2} g/cm 3 .

uncertainty of a factor of 2, which is probably overestimated. This induces an uncertainty of the same magnitude in the NEET rate because the reduced transition probability is a multiplicative factor in Eq. (5).

According to nuclear shell model calculations, the $5^- \rightarrow 6^-$ nuclear transition also has an $E2$ component with a weak, reduced transition probability [$B_{6^- \rightarrow 5^-}(E2) = 0.762$ W.u.] [43]. The corresponding $E2$ NEET rate is negligible in comparison to the $M1$ one as illustrated in Fig. 4, which represents the NEET rate calculated with ISOMEX as a function of the plasma temperature for the $M1$ and $E2$ components and for a density of $\rho = 10^{-2}$ g/cm 3 . In this work, the contributions of $E2$ transitions to the NEET rate based on MCDF calculations have therefore been neglected.

B. Evaluation of the plasma charge state distribution

For each plasma temperature and density there is a corresponding average charge state. In order to select the charge states contributing most to the NEET rate, we have calculated the ISOMEX excitation rates for average charge states lying between $\bar{Q} = 24^+$ and $\bar{Q} = 37^+$ at a plasma density of 10^{-2} g/cm 3 . Besides NEET, nuclear excitation by electron capture, photoexcitation, and inelastic electron scattering have been considered [10,16]. Figure 5 shows that NEET is the dominant excitation process for average charge states ranging from $\bar{Q} = 29^+$ to $\bar{Q} = 34^+$. Therefore only these charge states are considered in the MCDF calculations.

The charge state distribution required to evaluate a NEET rate [term P_Q in Eq. (16)] in an LTE ^{84}Rb plasma at a given temperature and density is obtained thanks to the FLYCHK code [44]. It is plotted in Fig. 6 for $T = 400$ eV and $\rho = 10^{-2}$ g/cm 3 . With these plasma characteristics, the ionic fraction P_Q of the Rb ions ranges from 29^+ to 34^+ , which corresponds to the charge states where the NEET process is dominant (see Fig. 5).

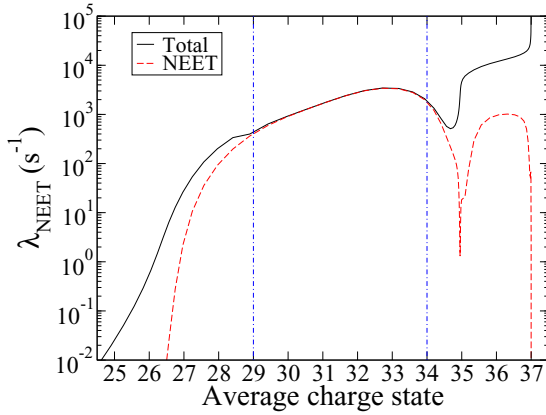


FIG. 5. ISOMEX total excitation rate (including photoexcitation, nuclear excitation by electron capture, and inelastic electron scattering) and NEET rate as functions of the average charge state in an ^{84m}Rb plasma at a density of 10^{-2} g/cm^3 .

C. Description of the atomic transitions involved in the NEET process

1. Determination of the atomic shells to consider in the calculations

To determine the number of shells required to describe the atomic configurations in plasma, ISOMEX computations were performed with different values of the maximal principal quantum number n_{max} , allowing atomic transitions between shells $n \in \llbracket 4, n_{\text{max}} \rrbracket$ to $n = 2$. Figure 7 presents the results of these calculations. It shows that the lower the plasma temperature, the higher the principal quantum number which must be considered to take into account all the transitions contributing to the NEET rate. For example, at $T = 270 \text{ eV}$ and $\rho = 10^{-2} \text{ g/cm}^3$, shells up to $n = 12$ must be considered, whereas at $T = 400 \text{ eV}$, shells up to $n = 6$ are sufficient. In this work, the electronic configurations have been described with shells up to $n = 8$.

The procedure based on RAAM calculations used to select the most probable atomic configurations at given plasma

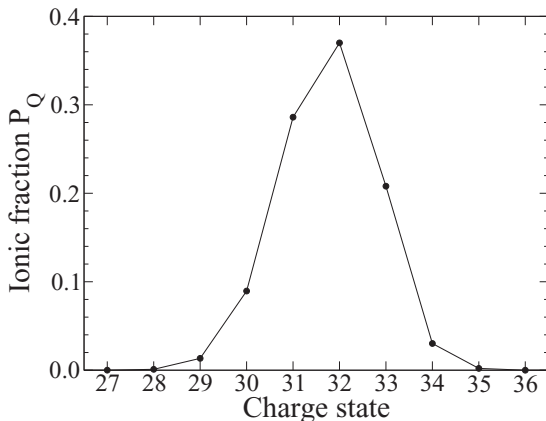


FIG. 6. Charge state distribution of an ^{84}Rb plasma at $T = 400 \text{ eV}$ and $\rho = 10^{-2} \text{ g/cm}^3$ calculated with the FLYCHK code under the LTE hypothesis [44].

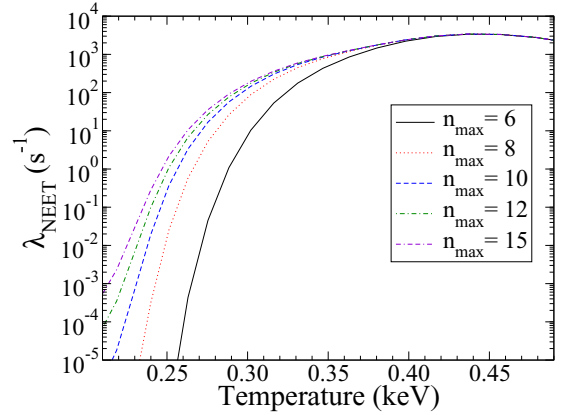


FIG. 7. NEET rate as a function of the plasma temperature for different values of the maximal principal quantum number used in the configuration description. The plasma density is 10^{-2} g/cm^3 .

temperature and density is described in detail in Ref. [12]. In that paper, it was used to calculate the x-ray spectra emitted by a Rb plasma. These spectra were compared to experimental ones. An excellent agreement was achieved, which validated the computation method.

2. Calculations of the atomic state widths in plasma

Calculation of the atomic state widths in plasma is a complex subject and dedicated codes have been developed for this purpose [45]. For our study, a fast evaluation of the state widths in an LTE plasma is required since many atomic states are considered in the NEET calculations. In the laser-produced plasma considered ($T = 400 \text{ eV}$, $\rho = 10^{-2} \text{ g/cm}^3$), the dominant line-broadening process is due to electron collisions. The collisional width of an electronic configuration can be expressed following the work of Baranger [46]. The sum $\Gamma_\alpha + \Gamma_\beta$ of the initial and final configuration widths of the $\alpha \rightarrow \beta$ transition is given by

$$\Gamma_\alpha + \Gamma_\beta = \alpha_{\text{FS}}^2 \hbar c \frac{4\sqrt{2}}{3\sqrt{3}} \pi^{3/2} n_e \sqrt{\frac{m_e c^2}{T}} \times (\langle \psi_\alpha | r^2 | \psi_\alpha \rangle + \langle \psi_\beta | r^2 | \psi_\beta \rangle), \quad (17)$$

where α_{FS} is the fine-structure constant, n_e is the plasma electronic density (in cm^{-3}), m_e is the electron mass, T is the plasma electronic temperature, r is the position operator, and $|\psi_\alpha\rangle$ is the wave function of subshell α : $|\psi_\alpha\rangle = |n_\alpha \kappa_\alpha j_\alpha m_\alpha\rangle$.

Evaluation of the atomic state widths is complex and we have considered several hypotheses. In our NEET calculations, we have supposed that the total atomic level width is equal to the total transition width: $\Gamma_i + \Gamma_f = \Gamma_\alpha + \Gamma_\beta$. This assumption is based on the fact that the energy of a level is only slightly different from the energy of the configuration used to build this level.

The calculations of the atomic widths with Eq. (17) for all lines determined by the MCDF lead to an average value of the characteristic time $\bar{\tau}_\infty = 0.7 \text{ ps}$ [see Eq. (1)]. The asymptotic value of the NEET probability is thus reached in a plasma produced with a nanosecond-pulse laser. The approximation

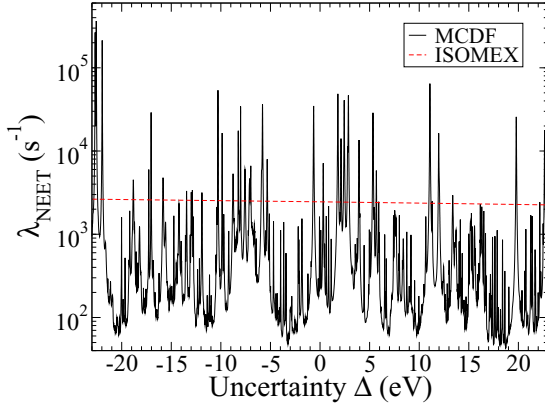


FIG. 8. $M1$ NEET rate as a function of the uncertainty Δ . Calculations with the MCDF and ISOMEX codes for a Rb plasma at $T = 400$ eV and $\rho = 10^{-2}$ g/cm³. Transitions between shells $n \in \llbracket 4, 8 \rrbracket$ to $n = 2$ for charge states ranging from $Q = 29^+$ to $Q = 34^+$ are considered.

consisting in taking into account only the asymptotic value of the NEET probability is therefore valid.

We assume an uncertainty of one order of magnitude in the atomic widths. According to Eq. (2) and if $\delta_{i1, f2} \rightarrow 0$, the impact of the atomic state width uncertainty is clearly visible. Indeed, if these widths are increased (decreased) by one order of magnitude, the peak value of the NEET rate is decreased (increased) by the same factor. However, far from resonance conditions, the influence of the widths on the NEET rate is reversed as the mismatch term in Eq. (2) becomes the dominant term in the denominator.

D. ^{84m}Rb NEET rate in a plasma at $T = 400$ eV and $\rho = 10^{-2}$ g/cm³

NEET is a resonant process which is very sensitive to the mismatch between the atomic and the nuclear transition energies. Therefore, one must take into account the uncertainties in these energies to obtain a realistic value of the NEET rate. To study the evolution of the NEET rate as a function of the mismatch uncertainty, the parameter Δ is introduced as in Refs. [16] and [32]:

$$\lambda_{\text{NEET}}(\Delta) = \sum_Q \sum_{i \rightarrow f} P_Q P_i^Q \frac{\Gamma_i + \Gamma_f}{\hbar} \times \frac{|R_{i1, f2}|^2}{(\delta_{i1, f2} + \Delta)^2 + \left(\frac{\Gamma_i + \Gamma_f}{2}\right)^2}. \quad (18)$$

The statistical uncertainty in the newly measured nuclear transition energy was evaluated as 6 eV at 1σ . The uncertainty in the atomic line energies were estimated as 5 eV in a comparison between theoretical and experimental x-ray spectra [12]. In the following, we consider a maximum variation of $\Delta = \pm 23$ eV which corresponds to an uncertainty at 3σ on the nuclear transition energy in addition to the atomic line energy uncertainty (5 eV).

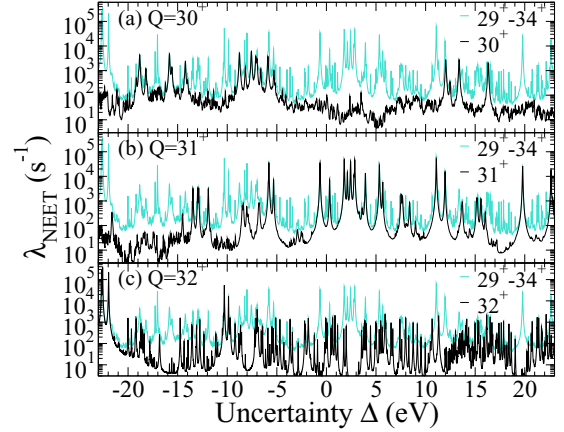


FIG. 9. $M1$ NEET rate as a function of the energy uncertainty Δ for an ^{84m}Rb plasma at $T = 400$ eV and $\rho = 10^{-2}$ g/cm³. The NEET rate of charge states (a) $Q = 30^+$, (b) $Q = 31^+$, and (c) $Q = 32^+$ and the total NEET rate (for $Q = 29^+$ to $Q = 34^+$) are plotted.

Figure 8 presents the evolution of the $M1$ NEET rates, calculated with the MCDF and ISOMEX, respectively, as functions of the uncertainty Δ .

According to MCDF calculations, the $M1$ NEET rate exhibits variations of several orders of magnitude in the energy uncertainty range considered. Indeed it is located in the range $4.4 \times 10^1 \leq \lambda_{\text{NEET}}^{M1} \leq 3.7 \times 10^5$ s⁻¹. The NEET rate calculated with the ISOMEX code is constant and does not reproduce the detailed structure of the MCDF NEET rate. This is a consequence of the average atom description implemented in this code: as the atomic line density is low, the average value calculated with ISOMEX is not representative of the NEET rate variations. Therefore in this case, this code can only be used to predict the general behavior of the NEET rate. It is not suitable for an accurate description of the NEET rate in an ^{84m}Rb plasma at the temperature and density considered.

In Fig. 9, the total NEET rate at $T = 400$ eV is shown for charge states $Q = 29^+$ to $Q = 34^+$ and one can see that charge states $Q = 30^+$ to $Q = 32^+$ contribute the most to the rate. This is consistent with the fact that these charge states are dominant in the plasma at 400 eV. At this temperature, the average plasma charge state is $\bar{Q} = 31.7$.

These transitions are from shells $n \in \llbracket 5, 7 \rrbracket$ to $n = 2$. As shown in Fig. 7, ISOMEX predicted that atomic shells with $n > 6$ contributed little to the global NEET rate. Figure 10 contradicts this conclusion by showing that transitions from $n = 7$ to $n = 2$ appear three times in the nine highest contributors to the MCDF-evaluated NEET rate.

E. Discussion

In this work, we have reduced by approximately one order of magnitude the uncertainty in the ^{84}Rb $5^- \rightarrow 6^-$ nuclear transition energy. It has been lowered to a level comparable to what is currently achievable in terms of atomic transition energy uncertainties in an MCDF approach with

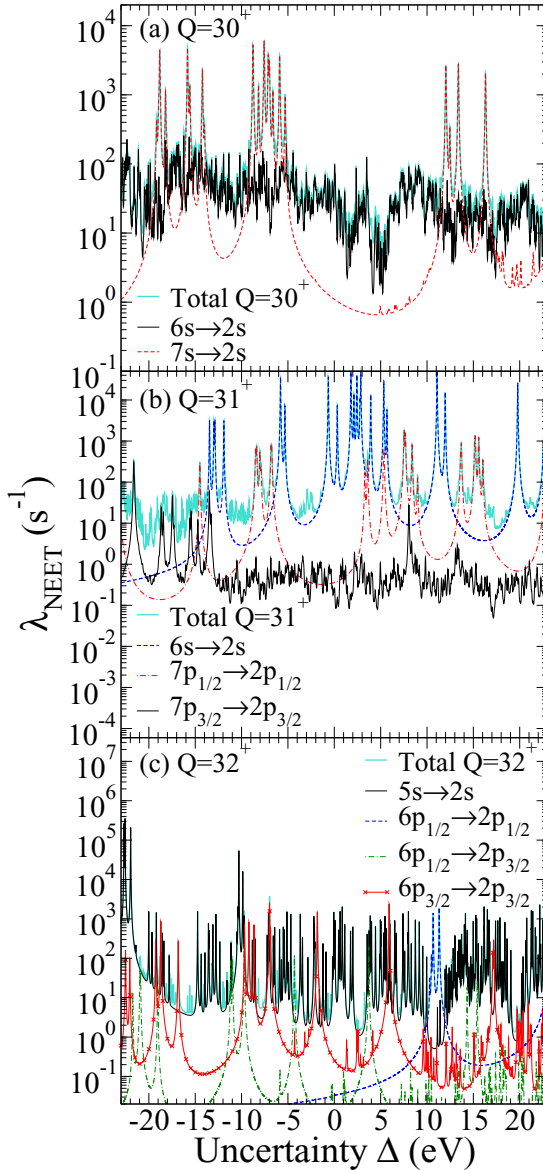


FIG. 10. $M1$ NEET rate for charge states (a) $Q = 30^+$, (b) $Q = 31^+$, and (c) $Q = 32^+$ as a function of the energy uncertainty Δ for an ^{84m}Rb plasma at $T = 400$ eV and $\rho = 10^{-2}$ g/cm 3 . The transitions which contribute the most to the total NEET rate for each charge state are indicated.

our treatment of the CI. A more accurate measurement of the nuclear transition energy is no longer necessary. However, the remaining uncertainties in the nuclear and atomic transition energies still lead to important variations of the NEET rate in the density and temperature region considered. Therefore only a range of NEET rates could be evaluated at these plasma temperatures and densities.

If we consider the uncertainties in the energy mismatch, the reduced transition probability, and the atomic state widths discussed above and summarized in Table II, we obtain the following NEET rate range at $T = 400$ eV and $\rho = 10^{-2}$ g/cm 3 : $2.2 \times 10^0 \leq \lambda_{\text{NEET}}^{M1} \leq 7.4 \times 10^6$.

TABLE II. Summary of the uncertainties used in the NEET rate computations.

Quantity	Value	Uncertainty
Atomic line energy	MCDF	5 eV at 1σ
Nuclear line energy	3.498 keV	6 eV at 1σ
Atomic line width	Eq. (17)	Factor 10
Reduced transition probability	0.08 W.u.	Factor 2

IV. CONCLUSION

The NEET rate excitation of the ^{84}Rb 6^- isomeric state has been evaluated in an LTE plasma at a temperature of 400 eV and a density of 10^{-2} g/cm 3 . The uncertainties in the different experimental and theoretical quantities involved in the calculations have been estimated. The MCDF NEET rates have been compared to the ISOMEX ones. ISOMEX does not reproduce the detailed structure of the MCDF NEET rates for the rubidium plasma considered in this work. Furthermore, although ISOMEX predictions correctly show the temperature or charge state range where the NEET rate is at its highest, its detailed predictions of which atomic transitions contribute should not be taken at face value but must be more thoroughly investigated.

In the MCDF NEET rate computations presented in this paper, a simple treatment of the CI has been performed due to computational limitations. The CI in the nonrelativistic configuration method could be used to obtain more accurate NEET rates. Indeed, the CI not only enriches the x-ray spectra but also has an impact on the atom-nucleus matrix element and therefore on the NEET rate.

The high-repetition rate and shorter pulse lasers under development such as Apollon [47] and ELI [48] may be an interesting alternative to study nuclear excitations in plasma. To use the model reported in this paper, we will have to reassess the relevance of using the asymptotic expression of the NEET probability as well as to devise a new evaluation of the charge states and configuration probabilities.

ACKNOWLEDGMENTS

We would like to thank N. Smirnova for the shell-model calculations. We gratefully acknowledge helpful discussions with O. Peyrusse, J.-C. Pain, and F. Gilleron. We would also like to thank the ELSA accelerator and Orsay Tandem crews for their help during the experiments. This work was supported by Région Aquitaine Contracts No. 20071304005 and 20111603003.

APPENDIX: EXPRESSION OF THE SQUARED ATOM-NUCLEUS COUPLING MATRIX ELEMENT IN THE $|JM\Pi\rangle$ STATE BASIS

1. Expression of the atom-nucleus coupling matrix element

a. Expression in the orbital basis

The expression of the atom-nucleus matrix element in the orbital basis $|n\kappa jm\rangle$ has been published by several authors [8, 15, 27, 49]. In this basis, it is expressed for an atomic

transition between the initial state $|\Psi_{k1}\rangle$ and the final state $|\Psi_{k'2}\rangle$ as

$$\begin{aligned} W_{k1,k'2} &= \sum_{\pi=\{E,M\}} \sum_{LM} \langle \Psi_{k'2} | H_{LM}^{\pi} | \Psi_{k1} \rangle \\ &= \sum_{\pi=\{E,M\}} \sum_{LM} \langle n_{k'\kappa k'} j_{k'} m_{k'} | H_{LM}^{\pi} | n_{k\kappa k} j_k m_k \rangle \\ &\quad \times \langle I_2 M_2 | H_{LM}^{\pi} | I_1 M_1 \rangle, \end{aligned} \quad (\text{A1})$$

$$\begin{aligned} W_{k1,k'2} &= \sum_{\pi=\{E,M\}} \sum_{LM} (-1)^{M+1+I_2-M_2+m_{k'}+1/2} i \sqrt{4\pi} e(k_{12})^{L+1} \frac{\sqrt{(2L+1)(2j_k+1)(2j_{k'}+1)}}{L(2L+1)!!} \\ &\quad \times \begin{pmatrix} I_2 & L & I_1 \\ -M_2 & -M & M_1 \end{pmatrix} \begin{pmatrix} j_{k'} & L & j_k \\ -m_{k'} & M & m_k \end{pmatrix} \begin{pmatrix} j_{k'} & L & j_k \\ \frac{1}{2} & 0 & -\frac{1}{2} \end{pmatrix} \langle I_2 \| \mathcal{M}(\pi L) \| I_1 \rangle M_{k'k}^e(\pi L), \end{aligned} \quad (\text{A2})$$

where $M_{k'k}^e(\pi L)$ is the electronic matrix element and $\mathcal{M}(\pi L)$ is the electromagnetic transition operator. The nuclear matrix element $\langle I_2 \| \mathcal{M}(\pi L) \| I_1 \rangle$ is linked to the reduced transition probability $B_{I_1 \rightarrow I_2}(\pi L)$ by

$$B_{I_1 \rightarrow I_2}(\pi L) = \frac{1}{2I_1 + 1} |\langle I_2 \| \mathcal{M}(\pi L) \| I_1 \rangle|^2. \quad (\text{A3})$$

b. Expression in the $|JM\Pi\rangle$ state basis

In the $|JM\Pi\rangle$ basis, the atom-nucleus matrix element between an initial $|\Psi_{i1}\rangle$ and a final $|\Psi_{f2}\rangle$ state is expressed as

$$\begin{aligned} W_{i1,f2} &= \sum_{\pi=\{E,M\}} \sum_{LM} \langle \Psi_{f2} | H_{LM}^{\pi} | \Psi_{i1} \rangle \\ &= \sum_{\pi=\{E,M\}} \sum_{LM} \langle J_f M_f | H_{LM}^{\pi} | J_i M_i \rangle \\ &\quad \times \langle I_2 M_2 | H_{LM}^{\pi} | I_1 M_1 \rangle, \end{aligned} \quad (\text{A4})$$

where $|J_i M_i\rangle$ and $|J_f M_f\rangle$ are the initial and final atomic states, respectively, and $|I_1 M_1\rangle$ and $|I_2 M_2\rangle$ are the initial and final nuclear states, respectively. Equations (A4) and (A1) are formally identical. But atomic shells k and k' in (A1) have been replaced by atomic states i and f in (A4).

where H_{LM}^{π} is the atom-nucleus interaction Hamiltonian for a πL electromagnetic transition, $|n_{k\kappa k} j_k m_k\rangle$ and $|n_{k'\kappa k'} j_{k'} m_{k'}\rangle$ are the initial and final atomic orbitals, respectively, and $|I_1 M_1\rangle$ and $|I_2 M_2\rangle$ are the initial and final nuclear states, respectively. The parities of the atomic and nuclear states are not specified, to lighten the notation.

In Eq. (A1), the point-nucleus approximation was considered to allow the separation between the nuclear $\langle I_2 M_2 | H_{LM}^{\pi} | I_1 M_1 \rangle$ and atomic $\langle n_{k'\kappa k'} j_{k'} m_{k'} | H_{LM}^{\pi} | n_{k\kappa k} j_k m_k \rangle$ parts [49]. If the long-wavelength limit is considered for the nuclear part, $W_{k1,k'2}$ is given by

The atomic part $\langle J_f M_f | H_{LM}^{\pi} | J_i M_i \rangle$ of Eq. (A4), can be written, after application of the Wigner-Eckart theorem, as

$$\begin{aligned} \langle J_f M_f | H_{LM}^{\pi} | J_i M_i \rangle &= (-1)^{J_f - M_f} \begin{pmatrix} J_f & L & J_i \\ -M_f & M & M_i \end{pmatrix} \\ &\quad \times \sum_{i't'} \sum_{kk'} c_{it} c_{f't'} a_{t'k'k} \langle n_{k'\kappa k'} j_{k'} | H_L^{\pi} | n_{k\kappa k} j_k \rangle. \end{aligned} \quad (\text{A5})$$

In Eq. (A5), we have introduced the decomposition of the atomic states [Eq. (4)], $|J_i M_i\rangle = \sum_{it} c_{it} |v_t J_t M_t\rangle$, and we have expressed the matrix element in the orbital basis [Eq. (6)], $\langle v_{t'} J_{t'} | H_L^{\pi} | v_t J_t \rangle = \sum_{kk'} a_{t'k'k} \langle n_{k'\kappa k'} j_{k'} | H_L^{\pi} | n_{k\kappa k} j_k \rangle$.

The atom-nucleus matrix element can be written as

$$\begin{aligned} W_{i1,f2} &= \sum_{\pi=\{E,M\}} \sum_{LM} \sum_{i't'} \sum_{kk'} (-1)^{J_f - M_f} \begin{pmatrix} J_f & L & J_i \\ -M_f & M & M_i \end{pmatrix} \\ &\quad \times c_{it} c_{f't'} a_{t'k'k} \langle n_{k'\kappa k'} j_{k'} | H_L^{\pi} | n_{k\kappa k} j_k \rangle \\ &\quad \times \langle I_2 M_2 | H_{LM}^{\pi} | I_1 M_1 \rangle. \end{aligned} \quad (\text{A6})$$

Upon introducing the expression obtained in the orbital basis [see Eq. (A2)], Eq. (A6) becomes

$$\begin{aligned} W_{i1,f2} &= \sum_{\pi=\{E,M\}} \sum_{LM} \sum_{i't'} \sum_{kk'} i (-1)^{J_f - M_f + M + I_2 - M_2 - j_k + 1/2} \sqrt{4\pi} e(k_{12})^{L+1} \frac{\sqrt{(2L+1)(2j_k+1)(2j_{k'}+1)}}{L(2L+1)!!} \\ &\quad \times c_{it} c_{f't'} a_{t'k'k} \begin{pmatrix} J_f & L & J_i \\ -M_f & M & M_i \end{pmatrix} \begin{pmatrix} I_2 & L & I_1 \\ -M_2 & -M & M_1 \end{pmatrix} \begin{pmatrix} j_{k'} & L & j_k \\ \frac{1}{2} & 0 & -\frac{1}{2} \end{pmatrix} \langle I_2 \| \mathcal{M}(\pi L) \| I_1 \rangle M_{k'k}^e(\pi L). \end{aligned} \quad (\text{A7})$$

2. Expression of the squared atom-nucleus coupling matrix element in the $|JM\Pi\rangle$ state basis

In the expression of the NEET probability, the element $|R_{i1,f2}|^2$ is defined as a sum over the final atomic and nuclear magnetic substates and an average over the initial ones of the squared matrix element $W_{i1,f2}$:

$$|R_{i1,f2}|^2 = \frac{1}{(2J_i + 1)(2I_1 + 1)} \sum_{M_1 M_2} \sum_{M_i M_f} |W_{i1,f2}|^2. \quad (\text{A8})$$

The selection rules for the $(3j)$ Wigner coefficients lead to the following expression for Eq. (A8):

$$|R_{i1,f2}|^2 = \sum_{\pi=\{E,M\}} \sum_L \frac{4\pi e^2}{(2J_i+1)(2I_1+1)} \frac{(k_{12})^{2L+2}}{[L(2L+1)!!]^2} |\langle I_2 \| \mathcal{M}(\pi L) \| I_1 \rangle|^2 \\ \times \left| \sum_{it'} \sum_{kk'} (-1)^{-j_k} \sqrt{(2j_k+1)(2j_{k'}+1)} c_{it'} c_{ft} a_{t'k'k} \begin{pmatrix} j_{k'} & L & j_k \\ \frac{1}{2} & 0 & -\frac{1}{2} \end{pmatrix} M_{k'k}^e(\pi L) \right|^2. \quad (\text{A9})$$

By introducing Eq. (A3), and the relation between the $(3j)$ Wigner and the Clebsh-Gordan coefficients, $\begin{pmatrix} j_{k'} & L & j_k \\ \frac{1}{2} & 0 & -\frac{1}{2} \end{pmatrix} = \frac{(-1)^{j_{k'}-L+1/2}}{\sqrt{2j_k+1}} \langle j_{k'} L \frac{1}{2} 0 | j_k \frac{1}{2} \rangle$, we obtain

$$|R_{i1,f2}|^2 = \sum_{\pi=\{E,M\}} \sum_L \frac{4\pi e^2}{2J_i+1} \frac{(k_{12})^{2L+2}}{[L(2L+1)!!]^2} B_{I_1 \rightarrow I_2}(\pi L) \left| \sum_{it'} \sum_{kk'} \sqrt{2j_k+1} c_{it'} c_{ft} a_{t'k'k} \langle j_{k'} L \frac{1}{2} 0 | j_k \frac{1}{2} \rangle M_{k'k}^e(\pi L) \right|^2. \quad (\text{A10})$$

Indeed, if only one πL transition is considered for the NEET process, the sum over π and L is reduced to only one term.

-
- [1] T. Carreyre, M. R. Harston, M. Aiche, F. Bourguine, J. F. Chemin, G. Claverie, J. P. Goudour, J. N. Scheurer, F. Attallah, G. Bogaert, J. Kiener, A. Lefebvre, J. Durell, J. P. Grandin, W. E. Meyerhof, and W. Phillips, First direct proof of internal conversion between bound states, *Phys. Rev. C* **62**, 024311 (2000).
- [2] M. Morita, Nuclear excitation by electron transition and its application to uranium 235 separation, *Prog. Theor. Phys.* **49**, 1574 (1973).
- [3] S. Kishimoto, Y. Yoda, M. Seto, Y. Kobayashi, S. Kitao, R. Haruki, T. Kawauchi, K. Fukutani, and T. Okano, Observation of Nuclear Excitation by Electron Transition in ^{197}Au with Synchrotron X-Rays and an Avalanche Photodiode, *Phys. Rev. Lett.* **85**, 1831 (2000).
- [4] I. Ahmad, R. W. Dunford, H. Esbensen, D. S. Gemmel, E. P. Kanter, U. Rütt, and S. H. Southworth, Nuclear excitation by electronic transition in ^{189}Os , *Phys. Rev. C* **61**, 051304 (2000).
- [5] S. Kishimoto, Y. Yoda, Y. Kobayashi, S. Kitao, R. Haruki, and M. Seto, Evidence for nuclear excitation by electron transition on ^{193}Ir and its probability, *Nucl. Phys. A* **748**, 3 (2005).
- [6] T. Saito, A. Shinohara, and K. Oozai, Nuclear excitation by electron transition (NEET) in ^{237}Np following K-shell photoionization, *Phys. Lett. B* **92**, 293 (1980).
- [7] G. Gosselin and P. Morel, Enhanced nuclear level decay in hot dense plasmas, *Phys. Rev. C* **70**, 064603 (2004).
- [8] P. Morel, V. Méot, G. Gosselin, D. Gogny, and W. Younes, Evaluation of nuclear excitation by electronic transition in ^{235}U plasma at local thermodynamic equilibrium, *Phys. Rev. A* **69**, 063414 (2004).
- [9] F. Kondev, Nuclear data sheets for $A = 84$, *Nucl. Data Sheets* **110**, 2815 (2009).
- [10] F. Gobet, C. Plaisir, F. Hannachi, M. Tarisien, T. Bonnet, M. Versteegen, M. M. Aléonard, G. Gosselin, V. Méot, and P. Morel, Nuclear physics studies using high energy lasers, *Nucl. Instrum. Methods Phys. Res., Sec. A* **653**, 80 (2011).
- [11] J. Bruneau, MCDF calculation of argon Auger process, *J. Phys. B* **16**, 4135 (1983).
- [12] D. Denis-Petit, M. Comet, T. Bonnet, F. Hannachi, F. Gobet, M. Tarisien, M. Versteegen, G. Gosselin, V. Méot, P. Morel, J.-C. Pain, F. Gilleron, A. Frank, V. Bagnoud, A. Blazevic, F. Dorchie, O. Peyrusse, W. Cayzac, and M. Roth, Identification of x-ray spectra in the Na-like to O-like rubidium ions in the range of 3.8–7.3 Å, *J. Quant. Spectrosc. Radiat. Transfer* **148**, 70 (2014).
- [13] D. Denis-Petit, *Excitations nucléaires dans les plasmas: le cas du ^{84m}Rb* , Ph.D. thesis, Université de Bordeaux 2014.
- [14] D. P. Grechukhin and A. A. Soldatov, Institute of Atomic Energy Report IAE-2706, Technical report (IAE, Świerk, Poland, 1976).
- [15] E. V. Tkalya, Nuclear excitation in atomic transitions (NEET process analysis), *Nucl. Phys. A* **539**, 209 (1992).
- [16] M. R. Harston and J. F. Chemin, Mechanisms of nuclear excitation in plasmas, *Phys. Rev. C* **59**, 2462 (1999).
- [17] M. R. Harston, Analysis of probabilities for nuclear excitation by near-resonant electronic transitions, *Nucl. Phys. A* **690**, 447 (2001).
- [18] M. L. Goldberger and K. M. Watson, *Collision Theory* (Wiley, New York, 1964).
- [19] A. Ya. Dzyublik, Photo-induced nuclear excitation by electron transition, *JETP Lett.* **93**, 489 (2011).
- [20] A. Ya. Dzyublik, General theory of nuclear excitation by electron transitions, *Phys. Rev. C* **88**, 054616 (2013).
- [21] S. Kishimoto, Y. Yoda, Y. Kobayashi, S. Kitao, R. Haruki, R. Masuda, and M. Seto, Nuclear excitation by electron transition on ^{197}Au by photoionization around the k -absorption edge, *Phys. Rev. C* **74**, 031301 (2006).
- [22] J. P. Desclaux, The multiconfiguration Dirac-Fock method, *AIP Conf. Proc.* **189**, 265 (1989).
- [23] J. P. Desclaux, A multiconfiguration relativistic Dirac-Fock program, *Comput. Phys. Commun.* **9**, 31 (1975).
- [24] I. P. Grant, *Relativistic Quantum Theory of Atoms and Molecules. Springer Series on Atomic, Optical, and Plasma Physics*, Vol. 40 (Springer, Berlin, 2007).
- [25] I. P. Grant, Relativistic calculation of atomic structures, *Adv. Phys.* **19**, 747 (1970).
- [26] J. Mitroy and I. Morrison, A relativistic structure model for heavy atoms, *J. Phys. B* **17**, 4449 (1984).
- [27] Eugene V. Tkalya, Probability of l -shell nuclear excitation by electronic transitions in $^{178}\text{Hf}^{m2}$, *Phys. Rev. C* **68**, 064611 (2003).

- [28] E. V. Tkalya, Theory of the nuclear excitation by electron transition process near the k edge, *Phys. Rev. A* **75**, 022509 (2007).
- [29] D. Salzman, *Atomic Physics in Hot Plasmas. The International Series of Monographs on Physics 97* (Oxford University Press, New York, 1998).
- [30] P. A. Chodash, J. T. Burke, E. B. Norman, S. C. Wilks, R. J. Casperson, S. E. Fisher, K. S. Holliday, J. R. Jeffries, and M. A. Wakeling, Nuclear excitation by electronic transition of ^{235}U , *Phys. Rev. C* **93**, 034610 (2016).
- [31] B. F. Rozsnyai, Relativistic Hartree-Fock-Slater calculations for arbitrary temperature and matter density, *Phys. Rev. A* **5**, 1137 (1972).
- [32] M. Comet, G. Gosselin, V. Méot, P. Morel, J.-C. Pain, D. Denis-Petit, F. Gobet, F. Hannachi, M. Tarisien, and M. Versteegen, Nuclear excitation by electron transition rate confidence interval in a ^{201}Hg local thermodynamic equilibrium plasma, *Phys. Rev. C* **92**, 054609 (2015).
- [33] G. Gosselin, V. Méot, and P. Morel, Modified nuclear level lifetime in hot dense plasmas, *Phys. Rev. C* **76**, 044611 (2007).
- [34] G. Gosselin, N. Pillet, V. Méot, P. Morel, and A. Ya. Dzyublik, Nuclear transition induced by low-energy unscreened electron inelastic scattering, *Phys. Rev. C* **79**, 014604 (2009).
- [35] G. B. Han, S. X. Wen, X. G. Wu, X. A. Liu, G. S. Li, G. J. Yuan, Z. H. Peng, P. K. Weng, C. X. Yang, Y. J. Ma, and J. B. Lu, High spin states and signature inversion in ^{84}Rb , *Chin. Phys. Lett.* **16**, 487 (1999).
- [36] R. Schwengner, G. Rainovski, H. Schnare, A. Wagner, F. Donau, A. Jungclaus, M. Hausmann, O. Iordanov, K. P. Lieb, D. R. Napoli, G. de Angelis, M. Axiotis, N. Marginean, F. Brandolini, and C. R. Alvarez, Magnetic rotation in ^{82}Rb and ^{84}Rb , *Phys. Rev. C* **66**, 024310 (2002).
- [37] J. Döring, G. Winter, L. Funke, L. Käubier, and W. Wagner, New isomers and states of $(\pi g_{9/2} \otimes \nu g_{9/2})$ parentage in ^{84}Rb , *Z. Phys. A* **338**, 457 (1991).
- [38] C. Plaisir, F. Hannachi, F. Gobet, M. Tarisien, M. M. Aléonard, V. Méot, G. Gosselin, P. Morel, and B. Morillon, Measurement of the $^{85}\text{Rb}(\gamma, n)^{84m}\text{Rb}$ cross-section in the energy range 10–19 MeV with bremsstrahlung photons, *Eur. Phys. J. A* **48**, 1 (2012).
- [39] D. C. Radford, ESCL8R and LEVIT8R: Software for interactive graphical analysis of HPGe coincidence data sets, *Nucl. Instrum. Methods Phys. Res., Sec. A* **361**, 297 (1995).
- [40] Y. Khazov, A. Radionov, and F. G. Kondev, Nuclear data sheets for $A = 133$, *Nucl. Data Sheets* **112**, 855 (2011).
- [41] M. J. Martin, Nuclear data sheets for $A = 152$, *Nucl. Data Sheets* **114**, 1497 (2013).
- [42] M. Honma, T. Otsuka, T. Mizusaki, and M. Hjorth-Jensen, New effective interaction for f_5pg_9 -shell nuclei, *Phys. Rev. C* **80**, 064323 (2009).
- [43] N. Smirnova (private communication).
- [44] H.-K. Chung, M. H. Chen, W. L. Morgan, Y. Ralchenko, and R. W. Lee, FLYCHK: Generalized population kinetics and spectral model for rapid spectroscopic analysis for all elements, *High Energy Density Phys.* **1**, 3 (2005).
- [45] A. Calisti, F. Khelifaoui, R. Stamm, B. Talin, and R. W. Lee, Model for the line shapes of complex ions in hot and dense plasmas, *Phys. Rev. A* **42**, 5433 (1990).
- [46] M. Baranger, General impact theory of pressure broadening, *Phys. Rev.* **112**, 855 (1958).
- [47] J. P. Zou, C. Le Blanc, D. N. Papadopoulos, G. Chériaux, P. Georges, G. Mennerat, F. Druon, L. Lecherbourg, A. Pellegrina, P. Ramirez *et al.*, Design and current progress of the Apollon 10 PW project, *High Power Laser Sci. Eng.* **3**, e2 (2015).
- [48] F. Neigota *et al.*, *Romanian Reports in Physics*, ELI-NP Technical Design Reports Supplement 2016, Vol. 68 (Publishing House of the Romanian Academy, 2016), pp. S37–S144.
- [49] W. D. Hamilton (ed.), *The Electromagnetic Interaction in Nuclear Spectroscopy* (North-Holland, Amsterdam, 1975).